JCI The Journal of Clinical Investigation

Pancreatic ductal adenocarcinoma progression is restrained by stromal matrix

Honglin Jiang, Robert J. Torphy, Katja Steiger, Henry Hongo, Alexa J. Ritchie, Mark Kriegsmann, David Horst, Sarah E. Umetsu, Nancy M. Joseph, Kimberly McGregor, Michael J. Pishvaian, Edik M. Blais, Brian Lu, Mingyu Li, Michael Hollingsworth, Connor Stashko, Keith Volmar, Jen Jen Yeh, Valerie M. Weaver, Zhen J. Wang, Margaret A. Tempero, Wilko Weichert, Eric A. Collisson

J Clin Invest. 2020;130(9):4704-4709. https://doi.org/10.1172/JCI136760.

Concise Communication | Oncology

Graphical abstract

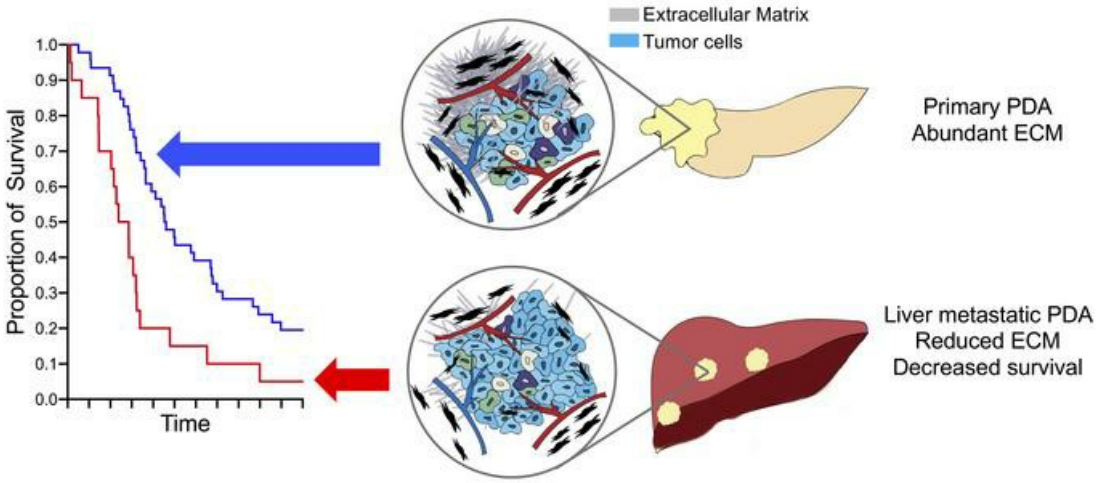

Pancreatic ductal adenocarcinoma progression is restrained by stromal matrix

Honglin Jiang,[1] Robert J. Torphy,[2] Katja Steiger,[3] Henry Hongo,[1] Alexa J. Ritchie,[1] Mark Kriegsmann,[4] David Horst,[5] Sarah E. Umetsu,[6] Nancy M. Joseph,[6] Kimberly McGregor,[7] Michael J. Pishvaian,[8,9,10] Edik M. Blais,[10] Brian Lu,[11] Mingyu Li,[11] Michael Hollingsworth,[12] Connor Stashko,[13] Keith Volmar,[14] Jen Jen Yeh,[15,16,17] Valerie M. Weaver,[13] Zhen J. Wang,[18] Margaret A. Tempero,[1] Wilko Weichert,[3] and Eric A. Collisson[1]

[1]Division of Hematology and Oncology, Department of Medicine and Helen Diller Family Comprehensive Cancer Center, UCSF, San Francisco, California, USA. [2]Department of Surgery, University of Colorado, Aurora, Colorado, USA. [3]Institute of Pathology, School of Medicine, Technical University Munich and German Cancer Consortium (DKTK; partner site Munich), Munich, Germany. [4]Department of Pathology, Institute of Pathology, Heidelberg University Hospital, Heidelberg, Germany. [5]Institute of Pathology, Charité - Universitätsmedizin Berlin, Berlin, Germany. [6]Department of Pathology, UCSF, San Francisco, California, USA. [7]Foundation Medicine, Cambridge, Massachusetts, USA. [8]Department of Oncology, Johns Hopkins University School of Medicine, Baltimore, Maryland, USA. [9]Sidney Kimmel Cancer Center, Johns Hopkins University School of Medicine, Washington, DC, USA. [10]Perthera, Inc, McLean, Virginia, USA. [11]Bristol-Myers Squibb, Summit, New Jersey, USA. [12]Eppley Institute for Research in Cancer and Allied Diseases, University of Nebraska Medical Center, Omaha, Nebraska, USA. [13]Center for Bioengineering and Tissue Regeneration, UCSF, San Francisco, California, USA. [14]Rex Healthcare, [15]Lineberger Comprehensive Cancer Center, [16]Department of Surgery, and [17]Department of Pharmacology, University of North Carolina, Chapel Hill, North Carolina, USA. University of North Carolina, Chapel Hill, North Carolina, USA. [18]Department of Radiology and Biomedical Imaging, UCSF, San Francisco, California, USA.

Desmoplasia describes the deposition of extensive extracellular matrix and defines primary pancreatic ductal adenocarcinoma (PDA). The acellular component of this stroma has been implicated in PDA pathogenesis and is being targeted therapeutically in clinical trials. By analyzing the stromal content of PDA samples from numerous annotated PDA data sets and correlating stromal content with both anatomic site and clinical outcome, we found PDA metastases in the liver, the primary cause of mortality to have less stroma, have higher tumor cellularity than primary tumors. Experimentally manipulating stromal matrix with an anti–lysyl oxidase like-2 (anti-LOXL2) antibody in syngeneic orthotopic PDA mouse models significantly decreased matrix content, led to lower tissue stiffness, lower contrast retention on computed tomography, and accelerated tumor growth, resulting in diminished overall survival. These studies suggest an important protective role of stroma in PDA and urge caution in clinically deploying stromal depletion strategies.

Introduction

Pancreatic ductal adenocarcinoma (PDA) is among the most lethal solid tumors and is projected to become the second-leading cause of cancer-related death in the United States by 2030 (1, 2). PDA is a heterogeneous and genetically diverse disease. Molecular PDA subtypes have been proposed (3–7) but do not yet drive clinical treatment decision making. Emerging studies implicate the tumor microenvironment as playing a pivotal role in tumor initiation, progression, and response to chemotherapy in conjunction with or independent from intrinsic alterations in tumor cells (4, 8). Identifying key prognostic or predictive features of the tumor stroma will facilitate useful stratification and possibly therapeutic selection tools for precision oncology efforts in this disease.

Notably, one such feature of PDA is the development of extensive fibrosis termed desmoplasia (9), with stromal components being more prevalent than pancreatic cancer cells. Tumor stroma has been considered to contribute to disease progression and therapeutic resistance in PDA and several mechanisms have been suggested (4, 10). However, recent studies have shown that stroma-depletion strategies can lead to more aggressive tumors in transgenic mouse models (11–13). Furthermore, several clinic trials targeting stroma (e.g., depleting hyaluronan) failed to achieve therapeutic benefit over standard-of-care chemotherapeutic approaches and may have been deleterious (14, 15). A more in-depth understanding of the role of stroma within the tumor microenvironment may provide new therapeutic strategies for improving patient survival.

In this study, we objectively assessed the amount of tumor stroma in clinical specimens of primary and metastatic PDA, hypothesizing that differences in tumor composition may translate into differences in patient survival. Further, we investigated the role of stroma in tumor development by depleting the extracellular matrix in experimental mouse models and examined the effects on tumor progression and therapeutic outcomes with standard-of-care agents.

Conflict of interest: KM is an employee of Foundation Medicine. MJP serves as a consultant for Perthera and holds stock in the company. EB is an employee of Perthera. BL is an employee of Bristol-Myers Squibb. ML is an employee and shareholder of Bristol-Myers Squibb. ZJW serves as a consultant for GE Healthcare. EC has Research Funding from Astra Zeneca, Ferro Therapeutics, Senti Biosciences, Merck KgA, and Bayer to UCSF; stock ownership in Tatara Therapeutics, Clara Health, BloodQ, Guardant Health, Illumina, Pacific Biosciences, and Exact Biosciences; and has received consulting income from Takeda and Merck.

Submitted: January 28, 2020; **Accepted:** May 29, 2020; **Published:** August 4, 2020.
Reference information: *J Clin Invest*. 2020;130(9):4704–4709.
https://doi.org/10.1172/JCI136760.

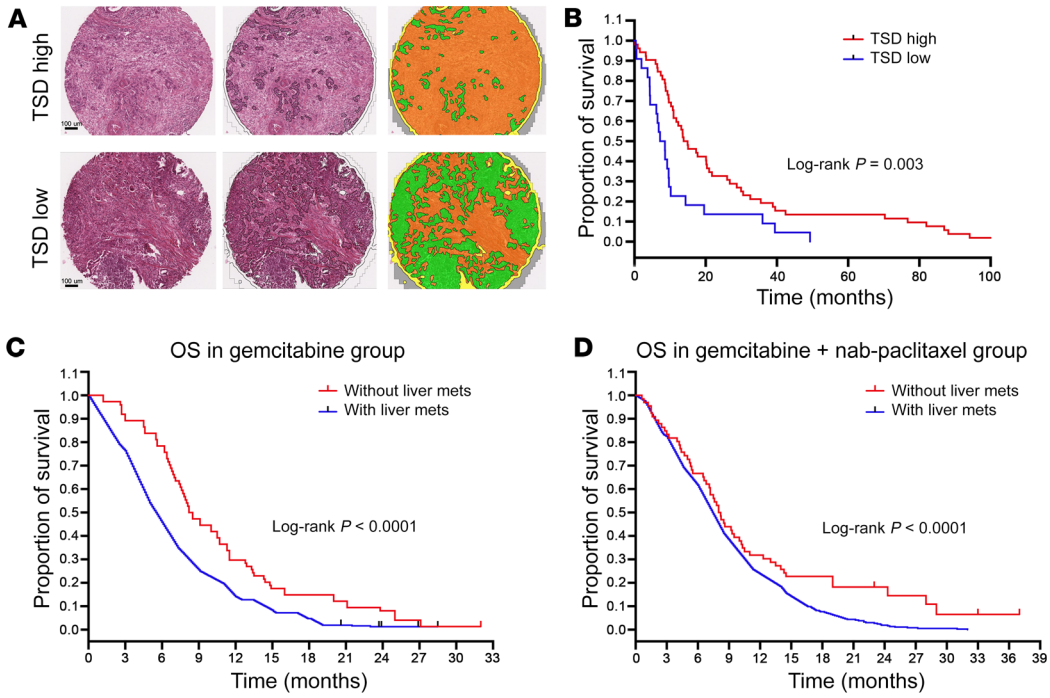

Figure 1. Low tumor stromal content correlates with worse patient survival. (**A**) Resected PDA specimens stained with H&E were segmented into tumor epithelium (green) and tumor stroma (yellow). Scale bars: 100 μm. (**B**) Kaplan-Meier curves of overall survival (OS) for high versus low tumor stromal density (TSD) in resected pancreatic adenocarcinoma (PDA) specimens from the Berlin patient cohort. Stratified by TSD from primary tumor, patients with high TSD had significantly longer OS than those with low TSD. (**C** and **D**) Kaplan-Meier survival analysis of patients with/without liver metastases (mets) from the MPACT study. Shorter OS was observed in patients with liver metastases in both the gemcitabine alone and gemcitabine plus nab-paclitaxel groups.

Results and Discussion

We previously demonstrated an automated method to assess the tumor stromal density (TSD) on hematoxylin and eosin–stained tissue microarray (TMA) slides and validated its use with multiple-pathologist stromal assessments (16). We performed automated TSD quantification on TMAs of primary resected tumors from 92 patients reported previously (17). Patient and clinicopathological characteristics as stratified by observed TSD are listed in Supplemental Table 1 (supplemental material available online with this article; https://doi.org/10.1172/JCI136760DS1). There were no apparent associations between TSD and patient gender, age, tumor grade, or disease stage. We next split the TMA cohort into low (<50% of core composed of stroma) and high (≥50% of core composed of stroma) TSD groups (Figure 1A). We found that the high TSD group enjoyed a longer survival than did the low TSD group using the Kaplan-Meier method (P = 0.036, Figure 1B). Further, in multivariable Cox regression analyses controlling for patient sex, age, T and N stage, overall stage, tumor grade, and surgical margins, low TSD was associated with impaired overall survival rate (HR = 2.19 [95% CI = 1.11–4.29], P = 0.022; Supplemental Table 2) in patients undergoing upfront tumor resection.

Liver metastasis is a common feature of PDA. More than 50% of patients with PDA have liver metastases at the time of diagnosis, but the stromal content of liver metastases has not been systematically studied. We analyzed patient characteristics from the MPACT trial that led to the current standard of care for metastatic PDA (18). We found liver metastases to be correlated with worse overall survival in 431 patients assigned to nab-paclitaxel plus gemcitabine and 430 patients assigned to gemcitabine alone (Figure 1, C and D). Because low stromal content correlates with poor prognosis, we next investigated the stromal signature in liver metastases using automated stroma quantification and collagen I immunofluorescence staining. Tissues from metastatic liver lesions described previously (7) had lower stromal content than did paired primary tumor specimens (mean TSD 23.1% versus 63.6%, P = 0.0045; Figure 2, A and B).

To further evaluate and characterize the stromal content of primary PDA and liver metastases in an independent patient cohort, we performed collagen I immunofluorescence staining on primary tumor and liver metastasis from samples collected under a rapid autopsy cohort (4). There was a significant correlation between TSD and collagen-positive tumor area across primary and metastatic samples (Spearman's correlation r = 0.69, P = 0.0155; Figure 2C). Analysis of collagen content in paired primary and metastatic liver sites also demonstrated increased collagen tumor area in primary tumors (59.75% collagen-positive tumor area) versus paired liver metastases (33.2% collagen-positive tumor area) (P = 0.0383, Figure 2D).

Because tumor cellularity reciprocally correlates with stromal content, we next expanded this observation to tumor molecular cellularity in large cohorts. We used mutant allele fractions across a multigene panel to assess tumor cellularity in samples from UCSF, UCLA, UCSD, and UC Davis sent to Foundation medicine for clinical next-generation sequencing (NGS). Tumor cellularity

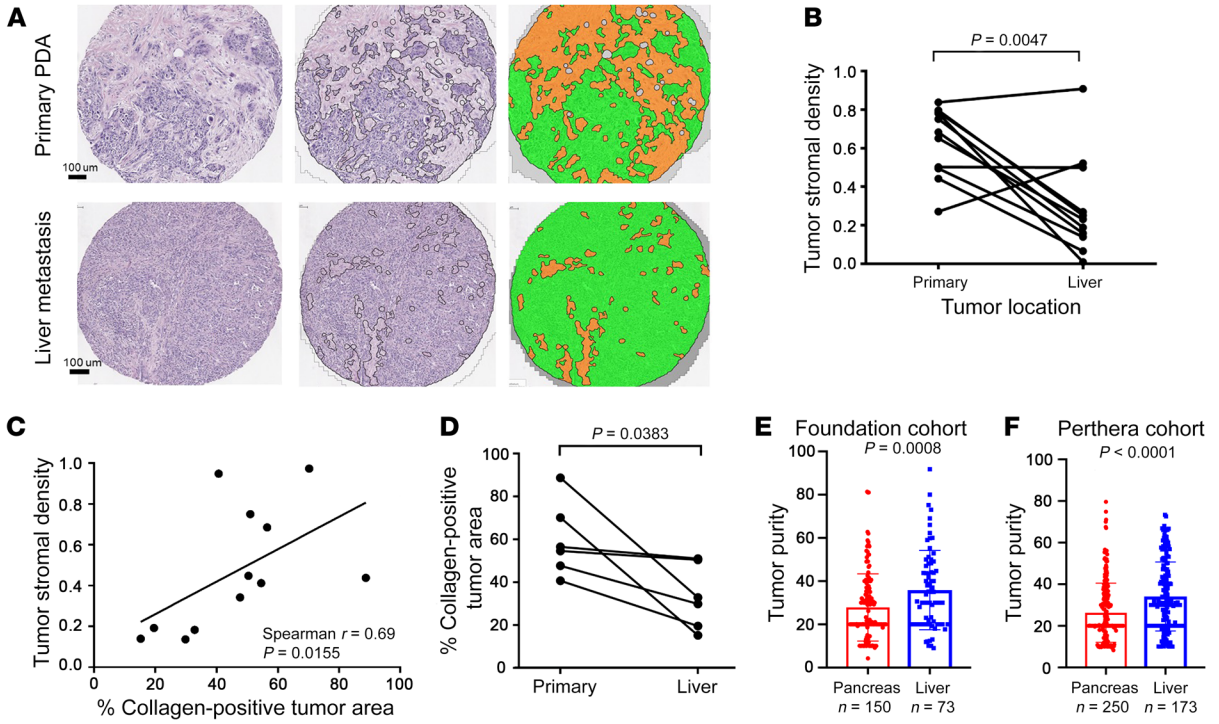

Figure 2. Stromal content varies in primary PDA tumors and liver metastases. (**A**) Representative images following automated tumor epithelial and stromal segmentation of H&E-stained primary PDA and liver metastasis (original magnification, ×10). Left: Unsegmented H&E sections. Middle and right: Segmented H&E sections (green = tumor epithelium; orange = stroma). (**B**) Tumor stromal density (TSD) was quantified in both primary PDA and paired liver metastases using automated tissue segmentation ($P = 0.0047$ by paired t test). (**C**) Correlation of automated TSD quantification and collagen immunofluorescence staining (percentage of tumor area) in primary PDA tissue and matched liver metastasis tissues (P value and correlation coefficient from Spearman's correlation paired t test, $P = 0.0383$). (**D**) Collagen content was quantified in both primary PDA and paired liver metastases using immunofluorescence staining. (**E** and **F**) Higher tumor cellularity in liver metastases compared with primary tumors was found in both the Foundation cohort ($P = 0.0008$ by unpaired t test) and the Know Your Tumor (Perthera) cohort ($P < 0.0001$ by unpaired t test).

was scored as a percentage and revealed a trend toward higher cellularity for liver lesions ($n = 73$, median = 35.1) versus primary pancreatic tumors ($n = 150$, median = 20, $P = 0.0008$; Figure 2E). In line with this finding, tumor cellularity from liver metastases ($n = 173$, median = 30) of an independent Know Your Tumor (19) cohort was significantly higher than that of the primary tumors ($n = 258$, median = 20, $P < 0.0001$; Figure 2F). Here, we observed variability of stromal content according to lesion site and the stromal content in primary tumors and liver metastases showed a strong negative correlation with overall survival in PDA patients.

To investigate the functional contribution of stromal content to PDA progression, we used a monoclonal antibody (mAb) that specifically recognizes lysyl oxidase like-2 (LOXL2) for in vivo stromal matrix depletion. Collagen cross-linking is an essential process for extracellular matrix stabilization. LOXL2 belongs to the lysyl oxidase (LOX) family of proteins encoding an extracellular copper-dependent amine oxidase that catalyzes the first step in the formation of cross-links in extracellular matrix components, including collagens and elastin. LOXL2 inhibition reduces collagen content and attenuates tissue fibrosis (20). We used an orthotopic murine PDA model to functionally test the effects of experimentally manipulating stromal content on tumor progression (Figure 3A). Hematoxylin and eosin (H&E) staining revealed an extensive reorganization of intratumoral collagen fibers with anti-LOXL2 mAb treatment (Figure 3B). Tumor collagen content assayed by trichrome staining was substantially decreased along with reduced stiffness in anti-LOXL2 mAb–treated tumors compared with control tumors (Figure 3, C and D, $P < 0.0001$).

We used an orthotopic murine PDA model to reliably recapitulate clinical and histopathological features of the human disease. We used 2 different mouse PDA lines, p53 2.1.1 (3) and FC1245 (21), that were each isolated from a *Kras*$^{LSL\text{-}G12D/+}$; *Trp53*$^{LSL\text{-}R172H/+}$; *Pdx1-Cre* (KPC) mouse but in FVB and C57BL/6 genetic backgrounds. Anti-LOXL2 mAb AB0023 (30 mg/kg, intraperitoneally 2 times a week, Gilead) started 1 week after the implantation and was continued for another 3 weeks (Figure 3A). Vehicle (IgG control) was administered in parallel. In both orthotopic models, tumors treated with anti-LOXL2 mAb presented with significantly increased bioluminescence signals compared with IgG-treated control tumors ($P < 0.05$ in FC1245 tumors and $P < 0.01$ in p53 2.1.1 tumors; Figure 4, A and B, and Supplemental Figure 1, A and B). Tumor weight was remarkably increased by anti-LOXL2 mAb treatment (Figure 4C and Supplemental Figure 1C).

PDA tissues with abundant stroma commonly show increased contrast enhancement/contrast retention at delayed-time-point CT. For the pattern of enhancement, the tumors were classified as having either low or high enhancement ratios. Figure 4D separately shows a representative image of a tumor in the IgG group classified as having a high normalized enhancement ratio and a representative tumor in the anti-LOXL2 treatment group that was

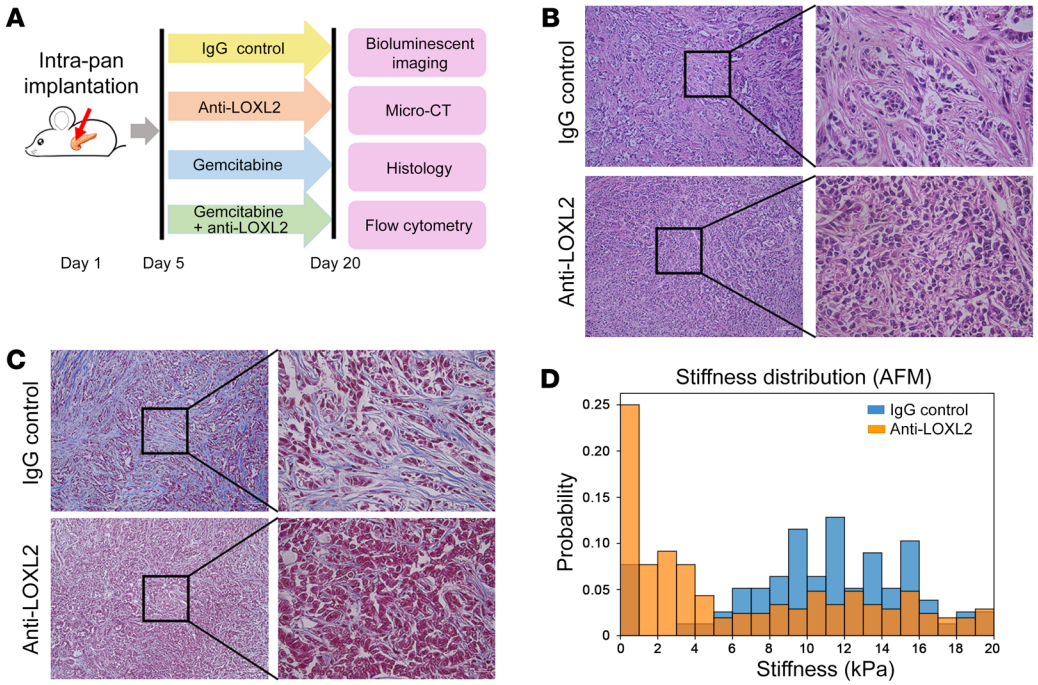

Figure 3. Anti-LOXL2 treatment abolished extracellular matrix in murine PDA model. (**A**) Schematic of the animal study. (**B** and **C**) H&E and trichrome staining revealed that intratumoral collagen fibers were notably reduced after anti-LOXL2 mAb. Original magnification, ×10 (left) and ×40 (right). (**D**) Anti-LOXL2–treated tumors had a stiffer extracellular matrix in the periductal region, as measured by atomic force microscopy (AFM).

classified as having a low normalized enhancement ratio. Tumors with normalized enhancement ratios of 0.32 or greater had significantly higher stromal content compared with those with normalized enhancement ratios less than 0.20 ($P = 0.01$, Figure 4D). In addition, we observed large amounts of ascites (Figure 4E) in anti-LOXL2–treated mice, indicating that stomal depletion promoted PDA development.

Delivery of small-molecule therapeutics may be hampered by stroma (22). To address the functional sequelae of stromal depletion in drug delivery, we next evaluated the effects of anti-LOXL2 mAb along with gemcitabine. We treated a separate cohort of mice with the combination of gemcitabine plus anti-LOXL2 mAb or gemcitabine plus IgG vehicle. Interestingly, in both orthotopic models, the addition of anti-LOXL2 to gemcitabine unexpectedly accelerated tumor progression (Figure 4, A and B, and Supplemental Figure 1, A and B) and resulted in slightly increased tumor weights at the endpoint (Figure 4C and Supplemental Figure 1C). These results suggest that any hypothetical benefit afforded by possible improved drug availability following stromal matrix depletion is outweighed by protumorigenic effects on the tumor itself.

To elucidate a potential causal link between the tumor biological behavior and the composition of epithelial and fibroblast compartments upon stromal matrix depletion, we flow sorted epithelial cells ($CD45^-EPCAM^+$) and fibroblasts ($CD45^-EPCAM^-PDGFR\alpha^+$) from tumors in both orthotopic models. In both FC1245 and p53 2.1.1 xenografts, there was a considerably increased proliferative capacity of tumor epithelial cells with the treatment of anti-LOXL2 mAb, as assessed by Ki67 signal (Supplemental Figure 2, A and B). We also observed a slightly lower percentage of fibroblasts in tumors from anti-LOXL2 mAb–treated mice (Supplemental Figure 2C), likely contributing to the aggressive phenotype of tumors upon anti-LOXL2 mAb treatment. As cancer-associated fibroblast (CAF) heterogeneity plays a vital role in PDA tumor biology (23, 24), we next sought to analyze the populations of myofibroblastic CAFs (myCAFs) and inflammatory CAFs (iCAFs). With flow cytometric analysis of several surface markers that distinguish the subset of iCAFs, we observed no significant difference in the percentage of either $\alpha SMA^{lo}IL\text{-}6^{hi}$ iCAFs (Supplemental Figure 2D) or $Ly6C^+$ iCAFs (Supplemental Figure 2E) in the tumors isolated from IgG- or anti-LOXL2 mAb–treated mice. Tumor-associated endothelial cells ($CD31^+$) were also equally distributed in tumors from IgG- or anti-LOXL2 mAb–treated mice, as was microvessel density (Supplemental Figure 2F). We then set out to determine the effect of stromal depletion on the immune infiltration. Tumors with stromal depletion presented with no significant changes in overall intratumoral infiltration of $CD45^+$ cells and $CD8^+$ T cells and $CD11b^+$ myeloid cells compared with control tumors (Supplemental Figure 3, A–D).

Stroma likely plays a dynamic and changing role over the course of tumorigenesis in the pancreas, estimated by some to last a decade or more (25), and its heterogeneous cellular and noncellular constituents change in relation to the evolving genetic landscape of cancer cells. In this regard, several studies have suggested that fibroblasts and type I collagen associated with tumor fibrosis are tumor promoting in solid tumors, including PDA (26–28). In this work, we have quantified the tumor stromal content in clinical PDA specimens from primary tumors and liver metastases using a variety of orthogonal methods with a convergent result enabling a generalizable conclusion. We find that low stromal infiltration of

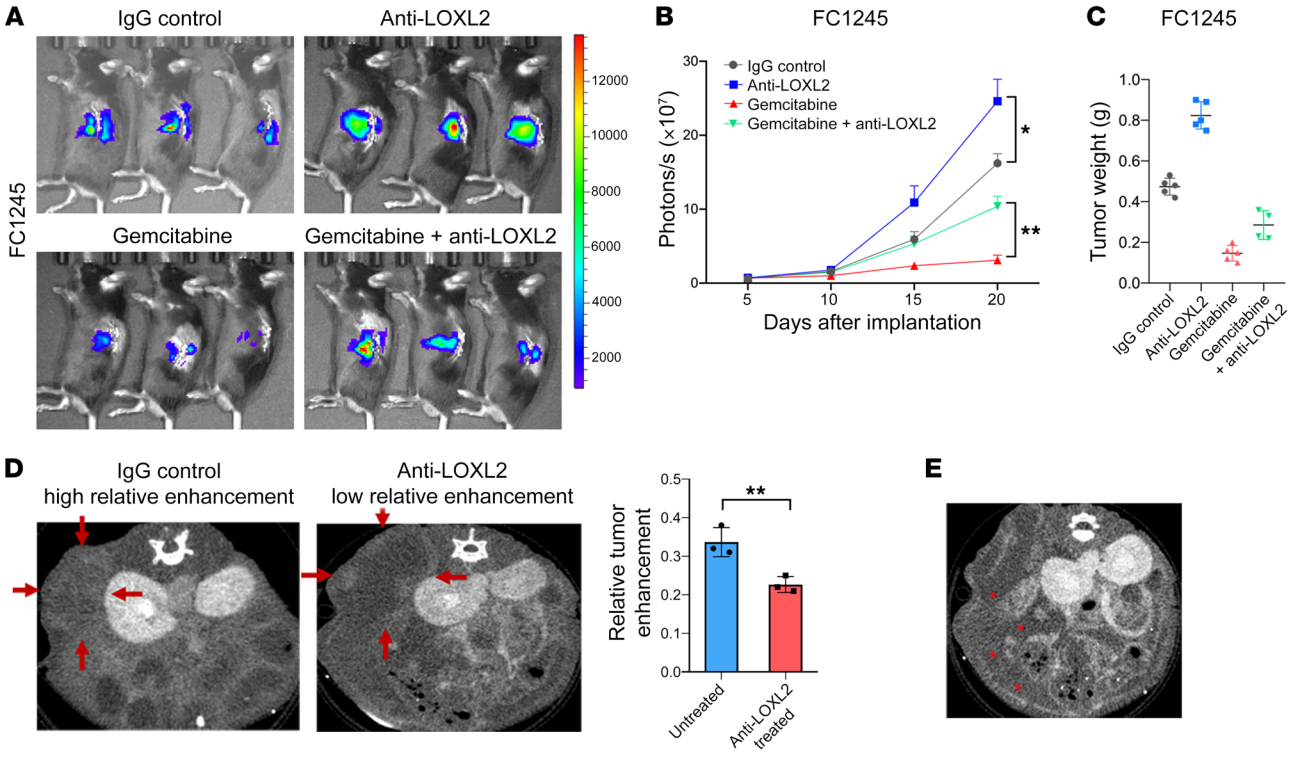

Figure 4. Reduction of fibrosis augments murine PDA progression. (**A**) Representative bioluminescence images of FC1245-fLuc orthotopic pancreatic tumor xenografts receiving IgG, anti-LOXL2 mAb, gemcitabine, or the combination of anti-LOXL2 mAb and gemcitabine. (**B**) Bioluminescent imaging signal changes (mean ± SEM) of FC1245 xenografts, n = 5 mice/group. Data were analyzed by 1-way ANOVA. $^*P < 0.05$; $^{**}P < 0.01$. (**C**) Tumor weight from **B** was measured at the endpoint. (**D**) Murine PDA tissues treated with anti-LOXL2 mAb showed relatively low enhancement compared with untreated tissue (P = 0.01). Red arrows indicate the region of interest. (**E**) Anti-LOXL2–treated mouse developed ascites, indicated with red asterisks.

the primary tumor was associated with shorter survival, and liver metastases had lower stromal infiltration using either automated, image-based methods or DNA sequencing–based methods. Furthermore, we show that pharmacologic depletion of stroma decreases tissue tension and in turn increases tumor aggressiveness in multiple, immunocompetent experimental mouse models. The simplest conclusion to be drawn from these convergent experimental models and clinical observations is that fibrosis (based on type I collagen) serves an important protective role in PDA that outweighs any hypothetical protumorigenic influence it may have on PDA tumor biology.

Although targeting of various stromal components and pathways (8, 22, 29) has shown benefits in improving drug delivery, inhibiting tumor growth and extending survival in preclinical mouse models, the clinical utility of this approach has not been established (13). In the context of our current findings, the large phase III studies combining pegylated human hyaluronidase (PEGH20) with either FOLFIRINOX or gemcitabine and nab-paclitaxel seemed to shorten overall survival in patients with metastatic PDA (14, 15).

We utilized a variety of retrospective data sets and paired primary versus liver metastasis specimens to ensure the robustness of our findings. However, prospective studies will be needed to further validate our conclusions. Moreover, stromal depletion was only performed by targeting one component (cross-linking of type I collagen via LOXL2 neutralization) of the extracellular matrix. As such, conclusions regarding other stroma-depletion techniques are indirect and further studies of other stroma-depleting components might yield differing results.

In summary, we examined variation in tumor stromal content in the primary tumor and liver metastases of PDA. We find important and reproducible differences in PDA tumors based on tumor stromal content as a function of anatomic site and identified low stromal content as an independent, poor prognostic factor. Syngeneic mouse PDA tumors with decreased stromal content are more aggressive, indicating that tumor stroma is a protective factor for PDA growth. This study highlights the complex interplay of tumor-stroma interactions and provides translational implications for future therapy for PDA patients.

Methods

Refer to Supplemental Methods for details.

Study approval. All animal experiments were performed in accordance with protocols approved by the UCSF Institutional Animal Care and Use Committee (IACUC).

Author contributions

HJ and EAC conceived of and designed the study. HJ, RJT, KS, MK, HH, AJR, DH, SEU, NMJ, KM, MJP, EMB, BL, ML, MH, WW, KV, JJY, and VMW were responsible for data collection. HJ, RJT, CS, ZJW, MAT, and EAC analyzed and interpreted the data. HJ, RJT, KS, and EAC wrote, reviewed, and/or revised the manuscript.

EAC supervised the study. All authors reviewed and approved the final manuscript as submitted and agree to be accountable for all aspects of the work.

Acknowledgments

The authors thank the University of North Carolina Translational Pathology Lab and the UC Davis Center for Genomic Pathology Lab & Center for Immunology and Infectious Diseases (CIID) for excellent technical assistance, and the Pancreatic Cancer Action Network for supporting the Know Your Tumor program and making the data available for this work. This work was supported by grants from the NCI/NIH (R01CA178015, R01CA227807, R01CA222862, and R01CA178015 to EAC), from the NIH (CA193650 and CA199064 to JJY), from the NIH/NCATS Colorado CTSA (TL1 TR002533 to RJT), and from the Deutsche Forschungsgemeinschaft (DFG, German Research Foundation, Project ID 329628492-SFB 1321; S02P to KS and WW). The content does not reflect the views of the funders.

Address correspondence to: Eric A. Collisson, 1450 3rd Street, San Francisco, California 94158, USA. Phone: 415.476.3659; Email: collissonlab@gmail.com.

1. Kleeff J, et al. Pancreatic cancer. *Nat Rev Dis Primers*. 2016;2:16022.
2. Ho CK, Rahib L, Liao JC, Sriram G, Dipple KM. Mathematical modeling of the insulin signal transduction pathway for prediction of insulin sensitivity from expression data. *Mol Genet Metab*. 2015;114(1):66–72.
3. Collisson EA, et al. Subtypes of pancreatic ductal adenocarcinoma and their differing responses to therapy. *Nat Med*. 2011;17(4):500–503.
4. Moffitt RA, et al. Virtual microdissection identifies distinct tumor- and stroma-specific subtypes of pancreatic ductal adenocarcinoma. *Nat Genet*. 2015;47(10):1168–1178.
5. Bailey P, et al. Genomic analyses identify molecular subtypes of pancreatic cancer. *Nature*. 2016;531(7592):47–52.
6. Puleo F, et al. Stratification of pancreatic ductal adenocarcinomas based on tumor and microenvironment features. *Gastroenterology*. 2018;155(6):1999–2013.e3.
7. Muckenhuber A, et al. Pancreatic ductal adenocarcinoma subtyping using the biomarkers hepatocyte nuclear factor-1A and cytokeratin-81 correlates with outcome and treatment response. *Clin Cancer Res*. 2018;24(2):351–359.
8. Olive KP, et al. Inhibition of Hedgehog signaling enhances delivery of chemotherapy in a mouse model of pancreatic cancer. *Science*. 2009;324(5933):1457–1461.
9. Mahadevan D, Von Hoff DD. Tumor-stroma interactions in pancreatic ductal adenocarcinoma. *Mol Cancer Ther*. 2007;6(4):1186–1197.
10. Knudsen ES, et al. Stratification of pancreatic ductal adenocarcinoma: combinatorial genetic, stromal, and immunologic markers. *Clin Cancer Res*. 2017;23(15):4429–4440.
11. Catenacci DV, et al. Randomized phase Ib/II study of gemcitabine plus placebo or vismodegib, a Hedgehog pathway inhibitor, in patients with metastatic pancreatic cancer. *J Clin Oncol*. 2015;33(36):4284–4292.
12. Özdemir BC, et al. Depletion of carcinoma-associated fibroblasts and fibrosis induces immunosuppression and accelerates pancreas cancer with reduced survival. *Cancer Cell*. 2014;25(6):719–734.
13. Lee JJ, et al. Stromal response to Hedgehog signaling restrains pancreatic cancer progression. *Proc Natl Acad Sci U S A*. 2014;111(30):E3091–E3100.
14. Hakim N, Patel R, Devoe C, Saif MW. Why HALO 301 failed and implications for treatment of pancreatic cancer. *Pancreas (Fairfax)*. 2019;3(1):e1–e4.
15. Doherty GJ, Tempero M, Corrie PG. HALO-109-301: a phase III trial of PEGPH20 (with gemcitabine and nab-paclitaxel) in hyaluronic acid-high stage IV pancreatic cancer. *Future Oncol*. 2018;14(1):13–22.
16. Torphy RJ, et al. Stromal content is correlated with tissue site, contrast retention, and survival in pancreatic adenocarcinoma [Published online January 16, 2018]. *JCO Precis Oncol*. https://doi.org/10.1200/PO.17.00121.
17. Noll EM, et al. CYP3A5 mediates basal and acquired therapy resistance in different subtypes of pancreatic ductal adenocarcinoma. *Nat Med*. 2016;22(3):278–287.
18. Von Hoff DD, et al. Increased survival in pancreatic cancer with nab-paclitaxel plus gemcitabine. *N Engl J Med*. 2013;369(18):1691–1703.
19. Pishvaian MJ, et al. Molecular profiling of patients with pancreatic cancer: initial results from the Know Your Tumor initiative. *Clin Cancer Res*. 2018;24(20):5018–5027.
20. Barry-Hamilton V, et al. Allosteric inhibition of lysyl oxidase-like-2 impedes the development of a pathologic microenvironment. *Nat Med*. 2010;16(9):1009–1017.
21. Roy I, et al. Pancreatic cancer cell migration and metastasis is regulated by chemokine-biased agonism and bioenergetic signaling. *Cancer Res*. 2015;75(17):3529–3542.
22. Provenzano PP, Cuevas C, Chang AE, Goel VK, Von Hoff DD, Hingorani SR. Enzymatic targeting of the stroma ablates physical barriers to treatment of pancreatic ductal adenocarcinoma. *Cancer Cell*. 2012;21(3):418–429.
23. Öhlund D, et al. Distinct populations of inflammatory fibroblasts and myofibroblasts in pancreatic cancer. *J Exp Med*. 2017;214(3):579–596.
24. Biffi G, et al. IL1-induced JAK/STAT signaling is antagonized by TGFβ to shape CAF heterogeneity in pancreatic ductal adenocarcinoma. *Cancer Discov*. 2019;9(2):282–301.
25. Yachida S, et al. Distant metastasis occurs late during the genetic evolution of pancreatic cancer. *Nature*. 2010;467(7319):1114–1117.
26. Karnoub AE, et al. Mesenchymal stem cells within tumour stroma promote breast cancer metastasis. *Nature*. 2007;449(7162):557–563.
27. Merika EE, Syrigos KN, Saif MW. Desmoplasia in pancreatic cancer. Can we fight it? *Gastroenterol Res Pract*. 2012;2012:781765.
28. Vong S, Kalluri R. The role of stromal myofibroblast and extracellular matrix in tumor angiogenesis. *Genes Cancer*. 2011;2(12):1139–1145.
29. Jacobetz MA, et al. Hyaluronan impairs vascular function and drug delivery in a mouse model of pancreatic cancer. *Gut*. 2013;62(1):112–120.